arXiv:1608.04038v1 [physics.flu-dyn] 13 Aug 2016

PREDICTION OF THE BED-LOAD TRANSPORT BY GAS-LIQUID STRATIFIED FLOWS IN HORIZONTAL DUCTS ☆ ,☆☆

Erick de Moraes Franklin

Faculdade de Engenharia Mecânica - Universidade Estadual de Campinas
e-mail: franklin@fem.unicamp.br
Rua Mendeleyev, 200 - Campinas - SP - CEP: 13083-970
Brazil

Abstract

Solid particles can be transported as a mobile granular bed, known as bed-load, by pressure-driven flows. A common case in industry is the presence of bed-load in stratified gas-liquid flows in horizontal ducts. In this case, an initially flat granular bed may be unstable, generating ripples and dunes. This three-phase flow, although complex, can be modeled under some simplifying assumptions. This paper presents a model for the estimation of some bed-load characteristics. Based on parameters easily measurable in industry, the model can predict the local bed-load flow rates and the celerity and the wavelength of instabilities appearing on the granular bed.

Keywords: Closed-conduit flow, pressure gradient, sediment transport, bed-load, instability

☆©2016. This manuscript version is made available under the CC-BY-NC-ND 4.0 license http://creativecommons.org/licenses/by-nc-nd/4.0/

☆☆Accepted Manuscript for Applied Mathematical Modelling, v. 37, p. 5627-5636, 2013, 10.1016/j.apm.2012.11.013

1. INTRODUCTION

Closed-conduit pressure-driven flows can entrain solid particles as a mobile granular bed, known as bed-load. Bed-load occurs when the shear stresses exerted by the fluid flow can displace some grains by rolling or sliding, but not as a suspension, forming then a mobile granular bed [1, 2, 3, 4]. A case frequently found in industry is the bed-load transport by stratified gas-liquid flows in horizontal ducts. Some examples are the stratified patterns appearing in the pumping of gas, oil and sand in petroleum pipelines and of gas, slurry and solid residues in sewage ducts.

In the presence of bed-load, the granular bed may be unstable, generating ripples and dunes. In a closed-conduit flow, these forms create supplementary pressure losses and pressure and flow rate transients [5, 6], so that a better knowledge of this kind of transport is of great importance to improve related industrial processes.

This three-phase flow, although complex, can be modeled under some simplifying assumptions. A model for the bed-load transport by stratified gas-liquid flows is proposed here for a case commonly found in industry, depicted in Fig. 1. The flow is pressure-driven in horizontal ducts, where the mean thickness of the granular layer h is many times smaller than that of the liquid layer $H-h$, and the mean thickness of the liquid layer $H-h$ is of the same order of magnitude as that of the gas $D-H$, i.e., $h/H \ll H/D = O(1)$. The thickness of the liquid layer is assumed to be much larger than the capillary length.

This paper presents a model valid for the specified case. The main purpose of the model is to predict, based on quantities easily measurable in industry, the local bed-load flow rates and the growth rate, the celerity and the wavelength of instabilities appearing on the granular bed.

The next section describes the physics and the main equations of the model. The following section describes the initial instabilities appearing on the granular bed and discusses their evolution to a saturated state. The conclusion section follows.

2. BED-LOAD IN A STRATIFIED GAS-LIQUID FLOW

The analyzed problem is very complex, so that the model's main objective is the estimation of the general behavior of the granular bed, adding new insights to it. In this case, the consideration of a three-dimensional geometry

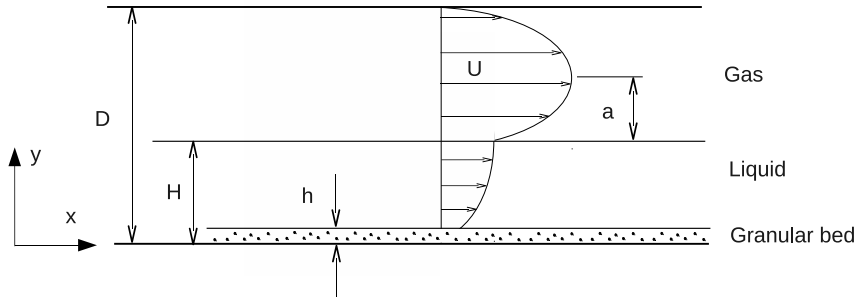

Figure 1: Granular bed sheared by a gas-liquid stratified flow. The thickness of the granular bed is h, that of the liquid layer is $H - h$, D is the duct height, U is the velocity of the mean flow in the longitudinal direction and a is the distance from the maximum of the velocity profile to the gas-liquid interface.

does not assure a better understanding of the problem: in a three-dimensional model, the obtained scaling laws and equations are more complex and depend on particular geometries, lacking generality. For this reason, the proposed model is two-dimensional.

The model divides the flow into a basic state, where the flow properties are homogeneous and steady in time, and a perturbation, which includes all the deviations from the basic state. This is described next.

2.1. Basic State

The flow can be divided in three layers, corresponding to the gas phase, to the liquid phase and to the granular bed. The basic state is considered as a steady state flow in which the thickness of each layer is constant in space and time. In the following, the variables in the basic state are identified by the subscript 0.

Equations relating interface shear stresses and pressure gradients can be found for the gas and liquid flows by integration of the momentum equation of the mean flow, as done by Cohen and Hanratty (1968) [7], for example. Then, a semi-empirical equation can be employed to estimate the bed-load flow rate.

Considering the basic state as a fully-developed incompressible flow, the integration of the y component of the mean flow momentum equation shows that the longitudinal pressure gradient does not vary in the x direction, in both the gas and liquid layers. In the gas, the momentum equation of the

mean flow in the x direction

$$0 = -\frac{1}{\rho}\frac{dP}{dx} - \frac{d\overline{u'v'}}{dy} + \nu\frac{d^2U}{dy^2} \tag{1}$$

can be integrated from $y = H_0$ to y, noting that at $y = H_0$ the interfacial stress is $\tau_{i,0} = \rho(-\overline{u'v'} + \nu dU/dy)$, and that at $y = (H_0 + a_0)$ the velocity reaches its maximum value, so that $dU/dy = 0$ and $\overline{u'v'} = 0$. In Eq. 1, ρ and ν are, respectively, the specific mass and the kinematic viscosity of the fluid, U is the velocity of the mean flow in the longitudinal direction, u' and v' are, respectively, the x and the y components of the velocity fluctuations, and $\overline{u'v'}$ is the stress tensor in the xy plane. The integration yields

$$\tau_{i,0} = a_0\left(-\frac{dp}{dx}\right) \tag{2}$$

In the liquid, Eq. 1 is integrated from the granular bed $y = h_0$, where the shear stress τ_0 is of viscous nature due to the the small values of fluctuations in this region, to the gas-liquid interface $y = H_0$. Considering that $O(h_0) < O(H_0)$, the integration yields

$$\tau_0 = (a_0 + H_0)\left(-\frac{dp}{dx}\right) \tag{3}$$

Equation 3 relates the shear stress on the granular bed to the pressure gradient (dp/dx) of the flow and to the position of the maximum $y = a_0$ of the velocity profile. These quantities are easily measurable, or can be estimated.

The pressure gradient can be measured by pressure transducers installed along the flow-line. However, if they are absent, the pressure gradient may be estimated by the Lockhart-Martinelli correlations for gas-liquid flows [8, 9]. These correlations, based on both the flow rates of the fluids and the gas fraction, were initially proposed for separated horizontal flows without phase change or significant acceleration. For this reason, they are applied here to horizontal stratified flows. In addition, they are relatively simple and have been largely employed and tested [10]. Basically, this method allows the estimation of the pressure gradient dp/dx for gas-liquid flows from the pressure gradient $(dp/dx)_g$ that would exist if pure gas flowed at the same mass flow rate

$$\frac{dp}{dx} = \phi_g^2 \left(\frac{dp}{dx}\right)_g \tag{4}$$

where the multiplied factor ϕ_g^2 may be determined from the mean gas fraction α in the duct. Chisholm (1967) [11] proposed, for both phases in turbulent regime,

$$\phi_g^2 = 1 + 20\left(\alpha^{-2.695} - 1\right)^{1.25} + \left(\alpha^{-2.695} - 1\right)^{2.5} \tag{5}$$

Equation 5 is valid for $Re_{ph} > 10^3$, where $Re_{ph} = \rho_{ph} j_{ph} D/\mu_{ph}$ is the Reynolds number of one phase, $j_{ph} = \dot{\forall}_{ph}/A_D$ is the volumetric flux, $\dot{\forall}_{ph}$ is the volumetric flow rate, A_D is the duct cross-section, μ_{ph} is the dynamic viscosity and the subscript ph indicates the phase.

The position of the maximum $y = a_0$ of the gas flow can be estimated as $a_0 \approx 0.5(D - H_0)$. For example, Cohen and Hanratty (1968) [7] found $0.4(D - H_0) < a_0 < 0.6(D - H_0)$ in their experiments.

In the basic state, the bed-load flow rate and the fluid flow are in equilibrium. In this case, called *saturated*, a semi empirical equation for the bed-load flow rate may be employed. Meyer-Peter and Mueller (1948) [12] performed exhaustive experiments in water flumes and obtained a widely used equation that is employed here

$$\frac{Q_0}{\sqrt{(S-1)gd^3}} = 8\left(\theta_0 - \theta_{th}\right)^{3/2} \tag{6}$$

where Q_0 is the bed-load flow rate, by unit of width, on the basic state, $S = \rho_s/\rho_l$ is the ratio of the specific masses of the solid ρ_s and the liquid ρ_l, d is the mean grain diameter, g is the gravitational acceleration and θ_0 is the Shields number in the basic state.

The Shields number θ is a dimensionless parameter characterizing the bed-load, defined as the ratio of the entraining force, scaling as $\tau_0 d^2$, to the resisting force, that scales with $(\rho_s - \rho_l)gd^3$

$$\theta = \frac{\tau}{(\rho_s - \rho_l)gd} \tag{7}$$

Bed-load takes place for $0.01 \lesssim \theta \lesssim 1$. The term θ_{th} corresponds to the Shields parameter at the bed-load threshold [4, 13, 14], and its value can be obtained by graphical charts or correlations [15, 16].

2.2. Perturbation

In the presence of bed-load, instabilities may appear on the surface of the granular bed, perturbing the fluid flow. The instabilities are bed undulations, initially of small aspect ratio, that grow and generate ripples and dunes [17]. Equations 3 and 6, obtained for the basic state, must then be corrected to take into account the perturbations. In the following, variables with the subscript *pert* are related to deviations from the basic state, and the ones without subscript are related to local values, i.e., the basic state added to the perturbation.

Franklin (2012) [18] obtained an expression for the shear stress on an undulated granular bed in the case of gravitational free-surface flows. His model supposed the existence of an outer region, far enough from the bed, where the perturbations induced by the bedforms had a relatively small length-scale, so that the turbulence could not adapt to the mean flow. With this assumption, the perturbation of the Reynolds stresses are negligible in this region and a potential solution shall exist at the leading order. Near the bed, on the other hand, the viscous effects and the shear stresses are important, however the flow perturbations are driven mainly by the pressure field of the outer region.

In the present model, it is assumed that the flow is turbulent and that $h/H \ll H/D = O(1)$, therefore an outer region is expected to exist. Near the bed the perturbations are driven by the pressure gradient of the outer region, so that the solutions obtained by [18] are valid and may be adapted to pressure driven flows. This is done next.

The shear stress on the undulated bed can be written as

$$\tau \;=\; \tau_0 \left(1 + \tau_{pert}\right) \tag{8}$$

where τ_0 is the shear stress on a flat bed (basic state) and τ_{pert} is the perturbation of the shear stress caused by the bed undulation. The shear stress perturbation τ_{pert} was found by [18] as

$$\tau_{pert} = f(Fr) A \left(\frac{h}{H_0} \;+\; B \partial_x h \right) \tag{9}$$

where $A = O(1)$ and $B = O(0.1)$ are constants and $f(Fr)$ is

$$f(Fr) = \frac{-1}{Fr^2 - 1} \tag{10}$$

where $Fr = U_0/\sqrt{gH_0}$ is the Froude number (the ratio between the velocity of the mean flow and the celerity of surface gravity waves) and U_0 is a characteristic velocity of the mean flow, considered here as the mean of the mean flow velocity profile, at the basic state. Equation 10 shows that $f(Fr)$ is constant for a given fluid flow.

With the shear stress given by Eq. 8, the saturated bed-load flow rate at the local flow conditions q_{sat} (by unit of width) can be computed employing the Meyer-Peter and Mueller (1948) [12] equation

$$\frac{q_{sat}}{\sqrt{(S-1)gd^3}} = 8\left(\theta - \theta_{th}\right)^{3/2} \tag{11}$$

which is similar to Eq. 6, but for the local conditions. However, the shear stress caused by the fluid on an undulated bed varies in space, as showed by Eqs. 8 and 9. Due to the inertia of the grains, the bed-load flow rate lags some distance (or time) to adapt to the local conditions of the fluid flow. This distance is a characteristic length called *saturation length*, L_{sat}. It was showed by [19, 20] that, in the case of liquid turbulent flows,

$$L_{sat} = \frac{u_*}{U_s} d \tag{12}$$

where $u_* = \sqrt{\tau_0/\rho_l}$ is the shear velocity and U_s is the settling velocity of one grain. A simplified expression taking into account this relaxation effect can be obtained from the erosion-deposition model of [14]

$$\frac{\partial q}{\partial x} = \frac{q_{sat} - q}{L_{sat}} \tag{13}$$

where q is the bed-load flow rate, by unit of width, on the undulated bed.

2.3. Bed-load estimation on pressure-driven gas-liquid flows

The local values of the bed-load flow rate can be computed employing the described equations. From the delivered gas and liquid flow rates, the pressure gradient can be estimated by Lockhard-Martinelli correlations (Eqs. 4 and 5). In cases where pressure transducers are installed along the line, the pressure gradient can be obtained directly from the measurements. In the basic state, the shear stress on the granular bed and the bed-load flow rate can be computed with Eqs. 3 and 6, respectively. If the granular bed is perturbed, the shear stress on the undulated bed can be computed with Eqs. 8 and 9 and the bed-load flow rate can be estimated with Eqs. 11 and 13.

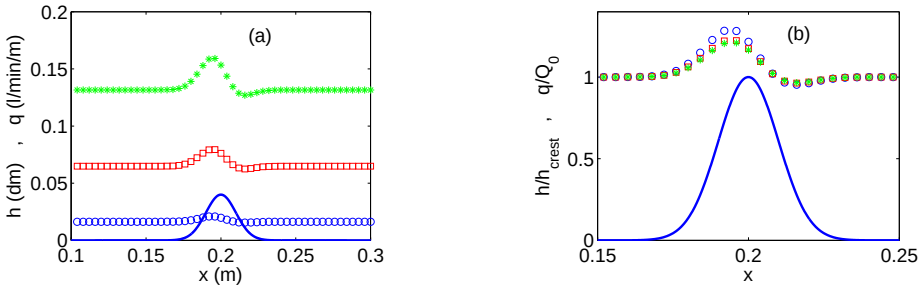

Figure 2: (a) Bedform height and bed-load flow rate as a function of the longitudinal position x. (a) Dimensional form and (b) dimensionless form. The continuous line correspond to the bedform height and the symbols to the bed-load flow rate. The circles correspond to $dp/dx = -4.3Pa/m$. The squares and asterisks correspond to $2dp/dx$ and $3dp/dx$, respectively.

In the latter case, however, computations require the form of the bed, i.e., the knowledge of the wavelength and of the amplitude of the bedforms. The determination of these values is presented in section 3. Next, assuming that the form of the bed is known, an example of calculation of the local bed-load flow rate is made.

Bed-load flow rates were estimated employing the following parameters: $d = 0.25mm$, $\rho_l = 10^3 kg/m^3$, $\mu_l = 10^{-3} Pa.s$, $\rho_g = 1.2kg/m^3$, $\mu_g = 2.10^{-5} Pa.s$, $\rho_s = 2600kg/m^3$, $D = 0.15m$, $H_0 = 0.35D$, $a_0 = 0.55(D - H_0)$ and $U_s = 0.01m/s$. The total longitudinal domain was $0.4m$ and the bedform was approximated by a Gaussian function, with an aspect ratio of 0.1, mean at $x = 0.2m$ and standard deviation of $S_d = 0.01m$. The value of the length of the bedform is then $L \approx 4S_d = 0.04m$, which is determined by the stability analysis of section 3 (cf. Tab. 2). Figure 2 summarizes the results of these computations, presenting the bed-load flow rate as a function of the longitudinal position x.

Figure 2(a) shows the bed-load flow rate q and the bedform height h as a function of the longitudinal position x, for three different pressure gradients. The continuous line corresponds to the bedform height h and the symbols to the bed-load flow rate. The circles correspond to $dp/dx = -4.3Pa/m$, estimated from $j_l = 0.1m/s$, $j_g = 3m/s$ and $\alpha = 0.65$. The squares and asterisks correspond to $2dp/dx$ and $3dp/dx$, respectively.

Far from the bedform, the bed-load flow rate is near the basic state and it is expected to vary as $(dp/dx)^{(3/2)}$. This is shown in the regions far from the crest of Fig. 2(a), where the values of q do not vary with x. In these

regions ($x < 0.15m$ or $x > 0.25m$) we find effectively that $q \sim (dp/dx)^{(3/2)}$. Over the bedforms, the variation of q depends also on the form of the bed because the fluid flow, which entrains the grains, is perturbed by it. This perturbation is taken into account via Eqs. 8 and 9, so that the relation between the bed-load and the pressure gradient in this region depends on the local slope of the bed.

Figure 2(b) presents the bed-load flow rate normalized by its value at the basic state q/Q_0 as a function of the longitudinal position x. The bedform height normalized by its maximum h/h_{crest} is also shown (continuous line). The symbols are the same as that of Fig. 2(a). From Fig. 2(b), it is clear that far from the bedform crest, where the bed is nearly flat, the bed-load flow rate is close to its saturated value Q_0.

Figure 2(b) also shows that the maximum of the bed-load flow rate occurs upstream of the bedform crest, which characterizes an unstable situation [20]: deposition occurs at the crest and the bedform amplitude tends to increase. This agrees with the analysis described in section 3, as the bedform length employed in computations was chosen as the most unstable mode (cf. Tab. 2). Just downstream of the bedform crest, due to smaller shear stresses in this region, the bed-load flow rate is smaller than the saturated value. This indicates that the perturbation caused by the imposed Gaussian form tends to accumulate grains at the crest and just downstream of it, so that the bedform tends to assume a triangular form with a gentle upstream slope and a rather abrupt downstream slope, just as observed in nature [1, 4, 3, 21].

Table 1 shows, for the computations presented in Fig. 2, the values of the bed-load flow rate at the basic state Q_0, the maximum local value of the bed-load flow rate q_{max}, the position where this maximum value occurs x_{max}, the value of the bed-load flow rate at the bedform crest q_{crest}, the minimum local value of the bed-load flow rate q_{min} and the position where this minimum value occurs x_{min}, in dimensional form. We verify that the maximum of the bed-load flow rate occurs slightly upstream of the bedform crest, and that a minimum value is reached downstream of the crest.

The values presented in Tab. 1 can be employed as initial estimations in the design of gas-liquid flow lines conveying grains as bed-load. To the author's knowledge, this is the first time that a model is proposed to give bed-load estimations as a function of the pressure gradient, which is an easily measurable parameter.

$-dp/dx$ (Pa/m)	Q_0 $(l/min/m)$	q_{max} $(l/min/m)$	x_{max} (m)	q_{crest} $(l/min/m)$	q_{min} $(l/min/m)$	x_{min} (m)
4.3	0.0163	0.0210	0.1940	0.0198	0.0155	0.2158
8.7	0.0649	0.0797	0.1942	0.0762	0.0624	0.2160
13.1	0.1316	0.1597	0.1944	0.1533	0.1270	0.2163

Table 1: Bed-load flow rate at the basic state Q_0, the maximum local value of the bed-load flow rate q_{max}, the position where this maximum value occurs x_{max}, the value of the bed-load flow rate at the bedform crest q_{crest}, the minimum local value of the bed-load flow rate q_{min} and the position where this minimum value occurs x_{min}, for different pressure gradients dp/dx.

3. STABILITY ANALYSIS

Fourière et al.(2010) [22] proposed, in the case of river streams, that ripples are primary linear instabilities while dunes are formed from the coalescence of ripples. Given the scope of the present model, the fundamental idea of [22] is employed here: ripples are bedforms whose wavelength does not scale with the flow depth and are formed as a primary linear stability, while dunes have a wavelength which scales with the flow depth and are formed as a secondary instability. The main difference here is that, given the scales of the liquid depth and that of ripples, dunes will be formed from a relative small quantity of ripples.

With this assumption, the initial instabilities give the scales of ripples. This is presented in subsection 3.1, where a linear stability analysis is made based on the equations presented in section 2. Subsection 3.2 discusses the nonlinearities and the formation of dunes.

3.1. Linear analysis

Franklin (2010) [20] presented a linear stability analysis of a granular bed sheared by a turbulent liquid flow, without free-surface effects. An analysis of the same kind is presented here, however, different from [20], the effects of the free surface as well as the bed-load threshold are taken into account. Also, as the interest here is in pressure-driven flows, the obtained equations are analyzed in terms of pressure gradients.

The linear analysis is based on four equations. The first one is the perturbation of the fluid flow by the shape of the bed, given by Eq. 9, which in the Fourier space is

$$\tilde{\tau}_{pert} \approx f(Fr) A_2 \tilde{h} \left[|k| + iBk \right] \tag{14}$$

as showed in [18], where k is the wavenumber in the longitudinal direction and the tilde denotes variables in the Fourier space.

The second equation is the saturated bed-load flow rate at the local flow conditions q_{sat}, given by Eq. 11. Here, different from [20], the flow is not assumed to be far from the threshold conditions ($\theta >> \theta_{th}$), so that the threshold term is conserved in the equation. Equation 11 can be linearized and made dimensionless by dividing it by a reference value, taken as the flow rate at the basic state. Considering the shear stress perturbation given by Eq. 14,

$$\frac{q_{sat}}{Q_0} \sim D_1 + \frac{3}{2} D_2 f(Fr) A_2 \left[|k| + iBk \right] h \tag{15}$$

where

$$D_1 = \left(1 - \frac{\tau_{th}}{\tau_0} \right)^{3/2} \tag{16}$$

$$D_2 = \left(1 - \frac{\tau_{th}}{\tau_0} \right)^{1/2} \tag{17}$$

and τ_{th} is the shear stress corresponding to θ_{th}. D_1 and D_2 are constants for a granular bed of a given granulometry under a given fluid flow. The great advantage of making the saturated bed-load flow rate dimensionless is to have an indication of how the normal modes shall be, as seen next.

The third employed equation is Eq. 13, that accounts for the relaxation effects related to the transport of grains, and the fourth one is the mass conservation of granular matter

$$\frac{\partial h}{\partial t} + \frac{1}{\varphi} \frac{\partial q}{\partial x} = 0 \tag{18}$$

where t is the time and φ is the solids concentration of the granular bed. Equations 13 and 18 are in the same form as in [20].

Taking into account that the initial instabilities are small scale perturbations, solutions to Eqs. 13, 14, 15 and 18 shall consider the bedform height h and the bed-load flow rate q as plane waves. Equation 15 indicates that h and q can be decomposed in normal modes of the form

$$h(x,t) \;=\; \xi e^{\sigma t - i\omega t + ikx} \tag{19}$$

$$\frac{q(x,t)}{Q_0} \;=\; D_1 + \gamma e^{\sigma t - i\omega t + ikx} \tag{20}$$

where σ is the growth rate and ω is the frequency. The insertion of the normal modes given by Eqs. 19 and 20 into Eqs. 13, 14, 15 and 18 gives origin to an eigenvalue problem

$$\left[\begin{array}{cc} \sigma - i\omega & (1/\varphi)ikQ_0 \\ (3/2)D_2\left(A_2|k| + iBk\right) & -(1+ikL_{sat}) \end{array} \right] \left[\begin{array}{c} \xi \\ \gamma \end{array} \right] = \left[\begin{array}{c} 0 \\ 0 \end{array} \right] \tag{21}$$

where $A_2 = f(Fr)A$ is constant for a given fluid flow. The non-trivial solution of Eq. 21 gives the growth rate and the frequency of initial instabilities. The group velocity corresponds to $c_G \;=\; d\omega/dk$,

$$\sigma \;=\; \frac{3}{2}\frac{D_2 Q_0}{\varphi}\frac{k^2\left(B - A_2|k|L_{sat}\right)}{1+\left(kL_{sat}\right)^2} \tag{22}$$

$$c_G \;=\; \frac{3}{2}\frac{D_2 Q_0}{\varphi}\frac{2A_2|k| + BL_{sat}k^2\left(3+\left(L_{sat}k\right)^2\right)}{\left(1+\left(kL_{sat}\right)^2\right)^2} \tag{23}$$

The form of Eq. 22, that can be seen in Fig. 3(a), shows that σ has a maximum that corresponds to a most unstable mode, which can then be found from $d\sigma/dk = 0$. In obtaining the most unstable mode, two approximations can be made: (i) the nature of the instability allows a long-wavelength approximation (Fig. 3), so that higher order terms in k can be neglected; and (ii) the value of A_2 can be considered as constant because the initial instabilities always happens at $Fr = O(0.1)$ in the analyzed case. With these assumptions, the most unstable wavenumber k_{max} is

$$k_{max} \;\approx\; \frac{2}{3}\frac{B}{A_2}\frac{1}{L_{sat}} \tag{24}$$

so that the wavelength λ_{max}, the growth rate σ_{max} and the celerity $c_{G,max}$ of the most unstable mode are

$$\lambda_{max} \;\approx\; \frac{3\pi A_2}{B}L_{sat} \tag{25}$$

$$\sigma_{max} \approx \frac{2}{3}\frac{D_2 Q_0}{\varphi}\frac{B^2}{A_2^2}\frac{1}{(L_{sat})^2} \tag{26}$$

$$c_{G,max} \approx 2B\frac{D_2 Q_0}{\varphi}\frac{1}{L_{sat}} \tag{27}$$

As the growth rate is exponential in the liner phase of the instability (Eqs. 19 and 20), the most unstable mode grows much faster than the others, so that it prevails. Initial bedforms appearing on the bed follow this mode and, as showed in [18, 23], they saturate, keeping the same wavelength. In pressure driven flows, it is then interesting to know how these forms vary with the pressure gradient dp/dx. From Eqs. 6, 12, 17, 25, 26 and 27

$$\lambda_{max} \sim \left(-\frac{dp}{dx}\right)^{(1/2)} \tag{28}$$

$$\sigma_{max} \sim \left(-\frac{dp}{dx}\right)^{(1/2)} \tag{29}$$

$$c_{G,max} \sim \left(-\frac{dp}{dx}\right) \tag{30}$$

Figure 3 presents the normalized growth rate σt_{ref} and the normalized celerity c_G/U_s of the initial bedforms as functions of the normalized wave-number kd, where $t_{ref} = d/U_s$ is the reference settling time. These values were computed from Eqs. 22 and 23 for five different pressure gradients: the circles correspond to $dp/dx = -4.3Pa/m$, estimated from $j_l = 0.1m/s$, $j_g = 3m/s$ and $\alpha = 0.65$. The squares, asterisks, crosses and triangles correspond to $2dp/dx$, $3dp/dx$, $4dp/dx$ and $5dp/dx$, respectively. The values of all other parameters, except the bedform, whose scales shall be found from this stability analysis, are the same as that employed in section 2.

Figure 3(a) shows that the large wave-numbers are stable and the small ones unstable, corresponding then to a long-wave instability. In the unstable region, the growth rate presents a maximum at a wave-number characterizing then the most unstable mode. The maxima of σ and the corresponding k and c_G were found from figure 3, and they were fitted as functions of dp/dx. The values found for the exponents of $-dp/dx$ related to λ, σ and c_G were 0.5, 0.6 and 1.1, respectively, showing a good agreement with Eqs. 28 to

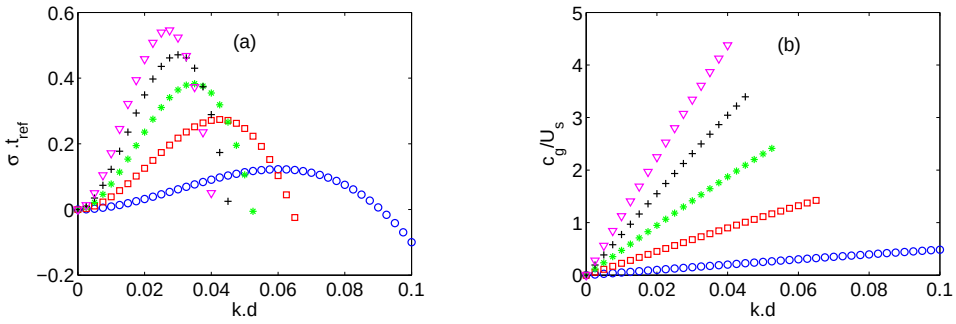

Figure 3: (a) Dimensionless growth rate σt_{ref} and (b) dimensionless celerity c_G/U_s of initial bedforms as functions of the dimensionless wave-number kd. The list of symbols is presented in Tab. 2.

30. This corroborates the long-wavelength assumption made in finding these equations.

Table 2 presents, for the most unstable mode, the wavelength λ_{max}, the celerity $c_{G,max}$ and the growth rate σ_{max} in dimensional form, for each pressure gradient dp/dx. These are the values expected to prevail in the linear phase of the instability. As we will see in the next subsection, this wavelength persists in the nonlinear phase, so that it can be employed in the estimation of the local bed-load flow rate by the method presented in section 2.

$-dp/dx$ (Pa/m)	Symbol $\cdots$	λ_{max} (m)	$c_{G,max}$ (m/s)	σ_{max} $(1/s)$
4.3	$\circ$	0.026	0.003	0.02
8.7	$\square$	0.037	0.010	0.05
13.1	$*$	0.045	0.017	0.07
17.4	$+$	0.052	0.023	0.09
21.8	∇	0.057	0.031	0.10

Table 2: Wavelength λ_{max}, celerity $c_{G,max}$ and growth rate σ_{max} of the most unstable mode for each pressure gradient dp/dx. The symbols employed in Fig. 3 are also listed.

To the author's knowledge, this is the first time that a model allows estimations of instabilities parameters as functions of the pressure gradient, which is an easily measurable quantity.

There is a lack of experiments in the scope of this model, even if there is a large number of industrial applications. However, the present model can

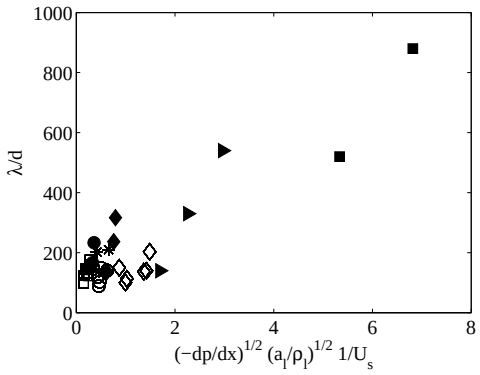

Figure 4: Dimensionless wavelength λ/d as a function of the dimensionless square root of the pressure gradient $(-dp/dx)^{1/2}(a_l/\rho_l)^{1/2}(1/U_s)$. Filled circles, lozenges, triangles and squares correspond to $d = 0.3mm$ and $\mu_l = 1cP$, $d = 0.3mm$ and $\mu_l = 2.2cP$, $d = 0.1mm$ and $\mu_l = 1cP$ and $d = 0.1mm$ and $\mu_l = 2.1cP$, respectively (experimental data of Kuru et al., 1995 [5]). Open lozenges, circles, squares and asterisks correspond to $d = 0.12mm$, $d = 0.20mm$ and $d = 0.50mm$ glass beads (in water) and to $d = 0.19mm$ zirconium beads (in water), respectively (experimental data of Franklin, 2008 [6])

be compared with experimental data of pressure driven liquid flows carrying grains as bed-load. Although the cases are different, the initial instabilities may scale in a similar manner, given that the initial bedforms have small amplitudes and are not expected to be affected by the presence of a free surface. There are at least two experimental works on bed instabilities under pressure driven closed-conduit flows: Kuru et al. (1995) [5] and Franklin (2008) [6]. Kuru et al. (1995) [5] performed experiments on a $7m$ long, $31.1mm$ diameter horizontal pipe, and employed mixtures of water and glycerin as the fluid media and glass beads as the granular media. Franklin (2008) [6] performed experiments on a $6m$ long, horizontal closed-conduit of rectangular cross-section ($120mm$ wide by $60mm$ high), made of transparent material, and employed water as the fluid and glass and zirconium beads as the granular media. In both works, the authors measured the wavelengths of the initial bedforms appearing on the granular bed. Given the small time scales of the problem and the presence of high uncertainties, the celerity and the growth rate were not reported.

The results of both works are summarized in Fig. 4. In order to directly compare the experimental data with the present model, Fig. 4 presents the

dimensionless wavelength λ/d of initial ripples as a function of the dimensionless square root of the pressure gradient $(-dp/dx)^{1/2}(a_l/\rho_l)^{1/2}(1/U_s)$, where a_l is the distance from the maximum of the liquid velocity profile to the bed. Filled symbols correspond to the experimental data of Kuru et al. (1995) [5] and open symbols to the experimental data of Franklin (2008) [6]. The description of each symbol is in the legend of Fig. 4.

The dimensionless parameters of Fig. 4 come from Eqs. 3, 12 and 25, considering that $u_* = \sqrt{\tau_0/\rho_l}$ and changing $(a_0 + H_0)$ by a_l. In this case, we find that

$$\frac{\lambda}{d} \sim \left(-\frac{dp}{dx}\right)^{1/2} \left(\frac{a_l}{\rho_l}\right)^{1/2} \frac{1}{U_s} \tag{31}$$

If we take into account the relatively high uncertainties, often present in measurements of bed instabilities, the alignment of the experimental data in Fig. 4 seems to support the results of the proposed model, that the wavelength of initial bedforms varies as $(-dp/dx)^{1/2}$, even if the experimental data were obtained for a case different from the scope of the model. This gives some confidence in the proposed model.

3.2. Considerations about nonlinearities

After the initial linear growth, bedforms attenuate their growth rate while keeping the same wavelength [23]. In the case of river streams, Franklin (2011) [18] showed that the initial bedforms saturate and generate ripples, which then coalesce and generate larger forms. These larger forms grow until the free surface is locally perturbed and the subcritical-supercritical transition is reached, so that the water stream becomes a stable mechanism. These forms, called dunes, maintain a wavelength in the range $H_0 \lesssim \lambda \lesssim 10H_0$ and are the result of a secondary instability, while ripples result from a primary instability.

The same reasoning can be applied to the present case. Given the dimensions of the problem it is expected that ripples saturate and that dunes are formed from their coalescence. The main difference in the present problem is that the number of coalesced ripples forming a dune is smaller than in rivers, and, depending on the flow depth, dunes can even be formed from a single ripple. In all cases, the dune length scales as

$$\lambda_{dune} \sim H_0 \tag{32}$$

Measured values indicate that $H_0 \lesssim \lambda \lesssim 10H_0$ [24, 25, 26, 27] in river flows. The celerity of dunes can be obtained from the mass conservation of grains (Eq. 18) together with Eq. 11. This gives an advection equation equal to the one obtained in [18], however with a different value for the celerity

$$c_{dune} \approx -\frac{24}{H_0(S-1)g}\left(\tau_0\right)^{\frac{3}{2}}\frac{1}{Fr^2-1} \tag{33}$$

and then, from Eq. 3, the celerity of dunes scales as

$$c_{dune} \sim \left(-\frac{dp}{dx}\right)^{(3/2)} \tag{34}$$

The model then predicts the coexistence of two different types of bedforms. The smaller type corresponds to ripples, whose length scales as $\lambda_{ripple} \sim (-dp/dx)^{(1/2)}$ and whose celerity scales as $c_{ripple} \sim (-dp/dx)$. The other type corresponds to dunes, that are larger forms scaling as $\lambda_{dune} \sim H_0$ and $c_{dune} \sim (-dp/dx)^{(3/2)}$. Depending on the flow depth, the length of saturated bedforms will obey Eq. 25 in subcritical flow, or $H_0 \lesssim \lambda \lesssim 10H_0$ otherwise. In any case, the bedforms grow until their crests reach a height corresponding to a local Froude number near the transition $Fr \approx 1$. This picture predicts that at development regions, such as the duct entrance, the granular bed and the fluid flow are adapting themselves so that ripples will be formed and predominate. In regions of fully-developed flow, the time and length scales are large enough to allow the growth of ripples and their coalescence, so that dunes will predominate.

Once determined the length and the amplitude of the bedforms, the local bed-load flow rates may be estimated by the method described in section 2. This justifies *a posteriori* the scales employed in the estimations of bed-load flow rates presented in section 2.

4. CONCLUSIONS

This paper presented a model for the estimation of bed-load and associated instabilities in stratified gas-liquid flows. The model focuses on the case of turbulent pressure-driven stratified flows, in horizontal closed-conduits. It divides the fluid flow and the bed-load into a flat basic state, and undulated perturbations. In order to compute the perturbations, the scales of the bed undulations are obtained by a stability analysis. The local shear stresses and bed-load flow rates are then the sum of the basic state and the perturbations.

The stability analysis predicted the coexistence of two different types of bedforms: the ripples, that are primary instabilities formed from the initial bedforms, and the dunes, that are secondary instabilities formed from the coalescence of ripples. Ripples predominate in development regions, such as the duct entrance, while dunes predominate in fully-developed regions of the flow.

The model can be employed to estimate bed-load flow rates and the shape of the bed in the design of lines of pressure-driven gas-liquid flows conveying grains. Other than the fluids and grains properties and the main geometry of the flow, the model needs the pressure gradient as an input. This quantity can be easily estimated or measured. To the author's knowledge, this is the first time that a model for a three-phase flow allows, from pressure gradient measurements, the estimation of instabilities parameters and bed-load flow rates.

5. ACKNOWLEDGMENTS

The author is grateful to Petrobras S.A. (contract number 0050.0045763.08.4) and to FAEPEX/UNICAMP (conv. 519.292, project 1435/12).

References

[1] R. A. Bagnold, The physics of blown sand and desert dunes, Chapman and Hall, 1941.

[2] R. A. Bagnold, The flow of cohesionless grains in fluids, Philos. Trans. R. Soc. Lond. Ser.A 249 (1956) 235–297.

[3] A. J. Raudkivi, Loose boundary hydraulics, 1st Edition, Pergamon Press, 1976.

[4] M. S. Yalin, Mechanics of sediment transport, 1st Edition, Pergamon Press, 1977.

[5] W. C. Kuru, D. T. Leighton, M. J. McCready, Formation of waves on a horizontal erodible bed of particles, Int. J. Multiphase Flow 21 (6) (1995) 1123–1140.

[6] E. M. Franklin, Dynamique de dunes isolées dans un écoulement cisaillé, Ph.D. thesis, Université de Toulouse (2008).

[7] L. S. Cohen, T. J. Hanratty, Effect of waves at a gas-liquid interface on a turbulent air flow, J. Fluid Mech. 31 (1968) 467–479.

[8] R. C. Martinelli, D. B. Nelson, Prediction of pressure drop during forced-circulation boiling of water, Trans. ASME 70 (1948) 695–702.

[9] R. W. Lockhart, R. C. Martinelli, Proposed correlation of data for isothermal two-phase, two-component flow in pipes, Chem. Eng. Prog. 45 (1949) 39–48.

[10] G. B. Wallis, One-dimensional two-phase flow, McGraw-Hill, 1969.

[11] D. Chisholm, A theoretical basis for the Lockhart-Martinelli correlation for two-phase flow, Int. J. Heat Mass Transfer 10 (1967) 1767–1778.

[12] E. Meyer-Peter, R. Mueller, Formulas for bed-load transport, in: Proc. 2nd Meeting of International Association for Hydraulic Research, 1948.

[13] J. M. Buffington, D. R. Montgomery, A systematic analysis of eight decades of incipient motion studies, with special reference to gravel-bedded rivers, Water Resour. Res. 33 (1997) 1993–2029.

[14] F. Charru, H. Mouilleron-Arnould, O. Eiff, Erosion and deposition of particles on a bed sheared by a viscous flow, J. Fluid Mech. 519 (2004) 55–80.

[15] R. J. S. Whitehouse, J. Hardisty, Experimental assessment of two theories for the effect of bedslope on the threshold of bedload transport, Marine Geology 79 (1988) 135–139.

[16] R. L. Soulsby, R. J. S. Whitehouse, Threshold of sediment motion in coastal enviroments, in: 13th Australasian Coastal and Engineering Conference and 6th Australasian Port and Harbour Conference, Christchurch, New Zealand, 1997, pp. 149–154.

[17] F. Engelund, J. Fredsoe, Sediment ripples and dunes, Ann. Rev. Fluid Mech. 14 (1982) 13–37.

[18] E. M. Franklin, Linear and nonlinear instabilities of a granular bed: determination of the scales of ripples and dunes in rivers, Appl. Math. Model. 36 (2012) 1057–1067.

[19] F. Charru, Selection of the ripple length on a granular bed sheared by a liquid flow, Physics of Fluids 18 (121508).

[20] E. M. Franklin, Initial instabilities of a granular bed sheared by a turbulent liquid flow: length-scale determination, J. Braz. Soc. Mech. Sci. Eng. 32 (4) (2010) 460–467.

[21] A. J. Raudkivi, Transition from ripples to dunes, J. Hydraul. Eng. 132 (2006) 1316–1320.

[22] A. Fourrière, P. Claudin, B. Andreotti, Bedforms in a turbulent stream: formation of ripples by primary linear instabilities and of dunes by nonlinear pattern coarsening, J. Fluid Mech. 649 (2010) 287–328.

[23] E. M. Franklin, Nonlinear instabilities on a granular bed sheared by a turbulent liquid flow, J. Braz. Soc. Mech. Sci. Eng. 33 (2011) 265–271.

[24] H. P. Guy, D. P. Simons, E. V. Richardson, Summary of alluvial channel data from flume experiments, U.S. Geol. Survey Prof. Paper 462-I (1966) 1–96.

[25] J. R. L. Allen, Physical processes of sedimentation, American Elsevier, 1970.

[26] P. Y. Julien, G. J. Klaassen, Sand-dune geometry of large rivers during floods, J. Hydraul. Eng. 121 (9) (1995) 657–663.

[27] S. E. Coleman, V. I. Nikora, S. R. McLean, T. M. Clunie, T. Schlicke, B. W. Melville, Equilibrium hydrodynamics concept for developing dunes, Physics of Fluids 18 (105104).